Applied Catalysis B: Environmental 245 (2019) 596–603

Contents lists available at ScienceDirect

Applied Catalysis B: Environmental

journal homepage: www.elsevier.com/locate/apcatb

Conjugated donor-acceptor polymer photocatalysts with electron-output "tentacles" for efficient hydrogen evolution

Zhi-An Lan, Wei Ren, Xiong Chen*,[1], Yongfan Zhang, Xinchen Wang*,[1]

State Key Laboratory of Photocatalysis on Energy and Environment, College of Chemistry, Fuzhou University, Fuzhou, 350116, PR China

ARTICLE INFO

Keywords:
Conjugated polymer
Photocatalysis
Hydrogen evolution
Electron-output "tentacles"
Artificial photosynthesis

ABSTRACT

The tunable structures and versatile properties for conjugated polymers (CPs) make them viable as a molecular platform for photocatalytic water splitting. Normally, structure design of polymer photocatalyst is focus on tuning its optical band structure or charge-separation ability, the importance of electron-output ability in photocatalytic process is always ignored. This study demonstrates a molecular engineering strategy by introducing an electron-output "tentacle" site, i.e. dibenzothiophene-*S,S*-dioxide (FSO) unit, into the polymer backbone to construct a series of donor-acceptor type conjugated polymer photocatalysts for efficient hydrogen evolution, which not only results in optimized light absorption ability and excellent exciton-separation, but also leads to the efficient electron-output ability. Detailed DFT calculations further theoretically confirm the vital role of FSO unit as an electron-output "tentacle" site.

1. Introduction

Conjugated polymers, featured by their sustainability, cost-effectiveness, processability and finely-tuned properties by versatile organic protocols [1–6], have been regarded as a new generation of photocatalysts to complement inorganic semiconductors [7–10] for water splitting. After a decade-long development, the most widely investigated conjugated polymer, polymeric carbon nitride (CN), has presented a quantum yield about 60% for photocatalytic hydrogen evolution [11–20]. Meantime, some other linear/cross-linked polymers, in which their molecular structure can be more rational designed by using different building blocks, are also employed as photocatalysts for water splitting [21–25]. Cooper's group first shows us a series of pyrene-based conjugated microporous polymers (CMPs) with tunable optical gaps in a wide range of 1.94–2.95 eV just by controlling the ratios of different monomers [26]. However, even for the most photocatalytic active sample CP-CMP10 with a suitable optical gap, it still exhibits a low hydrogen evolution rate (HER) of 17.4 μmol h^{-1} (10 mg Cat.). It is generally accepted that the primary steps in photocatalytic action of conjugated polymers are the absorption of light in correlation to excitons generation by π-π* transitions in conjugated molecule and excitons separation to drive the redox reactions. Therefore, the most probable reason for the limited HERs of those CMPs is that the suitable optical gap only affords a well exciton-generation ability, the photocatalytic performance still suffers a torpid exciton-separation efficiency in the polymer structure.

To realize a better exciton-separation efficiency, a donor (D)-acceptor (A) structure design protocol, which has already been widely used in organic photovoltaics (OPVs) [27,28], is also proposed to the synthesis of polymeric photocatalysts. In a D-A polymer, the inherently different electron affinities between donor and acceptor will lead to a large dipole moment in D-A backbone. During the photocatalytic action (see the Scheme 1a), this large dipole moment can trigger intramolecular charge transfer (ICT) from donor to acceptor in the excited state and the photoelectrons can be preferably concentrated into acceptor molecules, which would efficiently facilitate the separation of excitons. Finally, the electron concentrated acceptor building blocks will output the electrons to reduce the protons. According to this strategy, many successful works on photocatalysis by D-A conjugated polymers which using benzothiadiazole, triazine or some other heterocycles containing sp^2-hybridized nitrogen as acceptor have been gradually reported [29–35]. However, in view of the wide kinds of organic molecules, the rationally selecting efficient acceptor for D-A conjugated polymer to enhance photocatalytic hydrogen evolution performance has yet to be explored.

Recently, some researches point out that heteroatoms such as N and S in polymer may serve as reactive sites for the catalytic reaction [36,37]. In virtue of this clue, we propose to use the acceptor which has

* Corresponding authors.
E-mail addresses: chenxiong987@fzu.edu.cn (X. Chen), xcwang@fzu.edu.cn (X. Wang).
[1] http://wanglab.fzu.edu.cn.

https://doi.org/10.1016/j.apcatb.2019.01.010
Received 30 November 2018; Received in revised form 24 December 2018; Accepted 6 January 2019
Available online 08 January 2019
0926-3373/

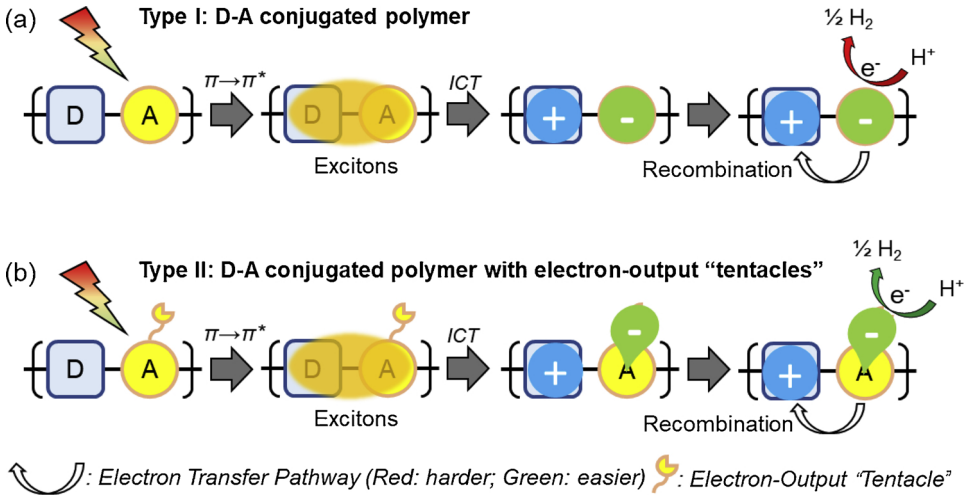

Scheme 1. Illustration of the photocatalytic processes in D-A conjugated polymers.

an electron-output "tentacle" to construct the D-A conjugated polymer. As shown in Scheme 1b, firstly, due to its strong electron affinity, this electron-output "tentacle" can withdraw and concentrate electrons from polymer; additionally, it also has a well interaction with co-catalyst or proton to efficiently output the electrons. Thus, in this type of D-A conjugated polymer, not only the excitons can be efficiently separated, but also the separated electrons can be greatly applied to drive the proton reduction reaction, resulting in a better chance of enhanced photocatalytic performance.

More recently, dibenzothiophene-*S,S*-dioxide (FSO) unit, which has been widely used in white polymer light-emitting diodes (WPLEDs) [38,39], has been selected as the candidate for the acceptor of D-A conjugated polymers and most of these FSO based polymers present the high efficiency for photocatalytic water splitting [40–43]. However, nearly no reports are focusing on the reason of excellent photocatalytic property caused by introducing FSO units as acceptor.

Herein, as shown in Fig. 1, we choose the well-known CP-CMP10 (noted as P-B in this paper) as the structural template to design a series of D-A conjugated polymers (Series 1) by gradually replacing the benzene units with FSO units for investigating the influence of FSO content in D-A conjugated polymers on their photocatalytic property. It is clearly observed that the higher FSO content in the polymer, the better hydrogen evolution rate can be realized. We hypothesize that this efficient photocatalytic performance is ascribed to the presence of sulphonyl group in FSO unit that can perfectly act as an electron-output "tentacle". To verify this hypothesis, two additional D-A conjugated polymers are further designed and synthesized (Series 2). P-FS employs dibenzothiophene (FS) to combine with pyrene, in which the sulphonyl group is absent. In P-FSOF, acceptor building block is replaced by the 2,8-difluorodibenzothiophene-*S,S*-dioxide (FSOF) which contains the sulphonyl group, but two additional strongly electrophilic F atoms are presented in the structure. A critical comparison between P-FSO and these two polymers in photocatalysis and combining with some theoretical study would then give us an insight into the effect of FSO units on the photocatalytic performance.

2. Experimental section

2.1. Materials

Anhydrous *N,N*-dimethylformamide (DMF), anhydrous tetrahydrofuran (THF), benzene-1,4-diboronic acid, 1,3,6,8-tetrabromopyrene, *n*-butyllithium solution (2.5 M in hexanes), [1,1′-bis(diphenylphosphino)ferrocene]dichloropalladium (II) (complex with

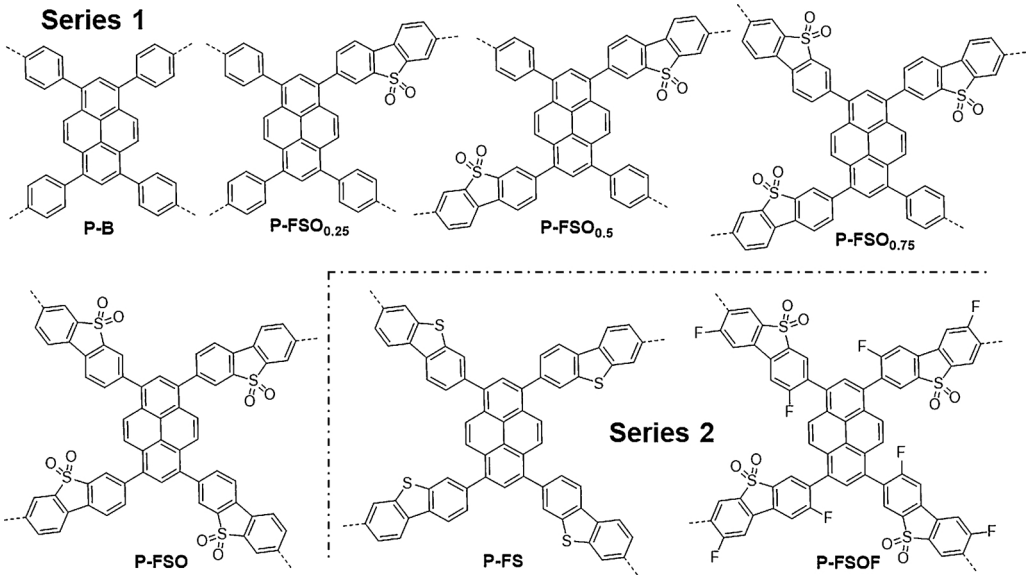

Fig. 1. Molecular structures of three series of D-A conjugated polymers.

dichloromethane), tetrakis(triphenylphosphine)palladium(0) (Pd(PPh_3)$_4$), potassium acetate, hydrochloric acid (37%), and sulfuric acid (95.0–98.0%) were purchased from Sigma-Aldrich. Dibenzothiophene 5,5-Dioxide, *N*-bromosuccinimide (NBS), bis(4-fluorophenyl) sulfone, 2,7-bis(4,4,5,5-tetramethyl-1,3,2-dioxaborolan-2-yl)pyrene, ammonium chloride, and potassium carbonate (K_2CO_3) were purchased from TCI. Bis(pinacolato)diboron, pyrene, lithium aluminum hydride, copper (II) bromide, and anhydrous copper (II) chloride were purchased from Alfa Aesar. 3,7-dibromodibenzothiophene-*S,S*-dioxide, 3,7-dibromodibenzothiophene, 3,7-bis(4,4,5,5-tetramethyl-1,3,2-dioxaborolan-2-yl)dibenzothiophene-*S,S*-dioxide, 2,8-difluorodibenzothiophene-*S,S*-dioxide, 3,7-dibromo-2,8-difluorodibenzothiophene-*S,S*-dioxide, 1,3,6,8-tetrakis(4,4,5,5-tetramethyl-1,3,2-dioxaborolan-2-yl)pyrene, 2,7-dibromopyrene were prepared according to reported methods [26,44–48].

2.2. Polymer synthesis

Suzuki-Miyaura cross-coupling reactions were carried out with a slight modification from the literature [26]. In a typical reaction, a flask was charged with the monomers, DMF, an aqueous solution of K_2CO_3 (2.0 M) and Pd(PPh_3)$_4$. The mixture was degassed and filled with Ar over 3 cycles and heated to 150 °C for 48 h. The mixture was cooled to room temperature and poured into water. The precipitate was collected by filtration and washed with water, ethanol and acetone. Further purification of the polymers was carried out by Soxhlet extraction with THF for 24 h and the product was dried under vacuum at 85 °C overnight. The detail of the synthesis for all polymers is given in the Supporting Information.

2.3. Sample characterizations

X-ray diffraction (XRD) measurements were performed on a Bruker D8 Advance diffractometer with Cu Kα1 radiation (λ = 1.5406 Å). The Fourier transform infrared (FTIR) spectra were recorded on a BioRad FTS 6000 spectrometer. The HITACHI SU8010 field emission scanning electron microscopy (SEM) was used to investigate the morphology of samples. X-ray photoelectron spectroscopy (XPS) data were obtained on Thermo ESCALAB250 instrument with a monochromatized Al Kα line source (200 W). UV–vis diffuse reflectance spectra (UV–vis DRS) were performed on Varian Cary 500 Scan UV–vis system. The photoluminescence (PL) spectra and time-resolved PL were acquired on an Edinburgh FI/FSTCSPC 920 spectrophotometer. Nitrogen sorption measurements were conducted at 77 K using Micromeritics ASAP 3020 equipment. The solid-state Cross-Polarization Magic Angle Spinning (CP/MS) ^{13}C NMR experiments were carried out on a Bruker Advance III 500 spectrometer.

2.4. DFT calculations

All density functional theory calculations were performed using Gaussian 03 program package [49]. The geometry optimizations and frequency calculations were carried out with the B3LYP hybrid functional and 6-31G* basis set while the electronic total energies were computed with additional single-point correction at B3LYP/6-311G** theory level. The average hydrogen adsorption free energies, for one adsorbed atom, have been calculated as follows:

$$\Delta G_H = G_{oligomer:H} - G_{oligomer} - (1/2)G_{hydrogen\_molecule}$$

where $G_{oligomer:H}$, $G_{oligomer}$ and $G_{hydrogen\_molecule}$ are the Gibbs free energies of the hydrogenated oligomer, pristine oligomer and hydrogen, respectively, with G=U + PV−TS [37]. The vibrational, rotational and translational contributions (statistical mechanics contributions) were included in the calculation of internal energy (U) and entropy (S), i.e., for instance, $U = E_{elect.} + ZPE + U_{vib}^{T} + U_{rot} + U_{trans}$ where ZPE and U_{vib}^{T} are the zero-point energy and vibrational contribution at finite temperature T, respectively [37]. The Pd adsorption free energies were calculated by the similar program.

2.5. Photocatalytic test

Photocatalytic hydrogen evolution arrays were conducted in a Pyrex top-irradiation reaction vessel linked to a sealed glass gas system. Hydrogen production was carried out by dispersing 50 mg of polymer powder in an aqueous solution (100 mL) containing triethanolamine (10 vol.%) as sacrificial electron donor. The reaction temperature was kept at 12 °C by cooling water. Before irradiation under a 300 W Xe-lamp with a long pass cut-off filter > 420 nm, the mixture was evacuated several times to remove air thoroughly. The generated gases were analyzed by gas chromatography with Argon as the carrier gas.

2.6. AQY measurement

The apparent quantum yields (AQYs) for hydrogen evolution were acquired using monochromatic LED lamps with band pass filter of 420, 450, 470, 490, 520 and 578 nm, the intensities were 9.7, 9.1, 5.9, 14, 5.5 and 2.2 mW cm^{-1}, respectively (Newport 2936-R optical power meter). The irradiation area was controlled as 9 cm^2. Depending on the amount of hydrogen produced by the photocatalytic reaction in one hour, and the AQYs have been calculated as follow:

$$AQY = 2\,M/N_p \times 100\%$$

where M is the amount of hydrogen molecules and N_p represents the incident photons.

3. Results and discussion

For preparing the polymers in Series 1, 1,3,6,8-tetrabromopyrene was firstly copolymerized with 1,4-benzene diboronic acid; then, different portion of 3,7-bis(4,4,5,5-tetramethyl-1,3,2-dioxaborolan-2-yl)dibenzothiophene-*S,S*-dioxide (FSO) was used to replace the 1,4-benzene diboronic acid: 0% (P-B), 25% (P-$FSO_{0.25}$), 50% (P-$FSO_{0.5}$), 75% (P-$FSO_{0.75}$) and 100% (P-FSO). The other two polymers in Series 2 were synthesized by polycondensation of 1,3,6,8-tetrakis(4,4,5,5-tetramethyl-1,3,2-dioxaborolan-2-yl)pyrene with the 3,7-dibromodibenzothiophene (P-FS) or 3,7-dibromo-2,8-difluorodibenzothiophene-*S,S*-dioxide (P-FSOF). All of the copolymerizations were conducted using Pd(0)-catalyzed Suzuki-Miyaura polycondensation. The detailed synthetic procedures are described in the Supporting Information.

All the polymers were obtained as insoluble solids and no crystallinity were observed from Powder X-ray diffraction (PXRD) patterns (Fig. S1). The chemical structures of these polymers were evidenced by FTIR spectroscopy, solid-state CP/MAS ^{13}C NMR spectroscopy, X-ray photoelectron spectroscopy (XPS) and elemental analysis in detail. As shown in FTIR spectra (Fig. 2a and b), the distinct skeleton vibration peaks of the aromatic ring can be clearly seen at 1456 and 1486 cm^{-1} for all polymers. The two strong peaks at 1310 and 1147 cm^{-1} for FSO/FSOF-containing polymers are the characteristic absorption of the sulphonyl group [50]. The solid-stated CP/MAS ^{13}C NMR spectroscopy (Fig. 2c and d) also confirms the presence of sulphonyl group (CSO_2, $\delta \approx 142$) in these polymers and it further evidences the presence of F (CF, $\delta \approx 162$) in P-FOSF [31]. The difference in the structure of the polymers were further unravelled by high-resolution XPS spectra (Fig. S2). The S species in P-FS found at 164.9 and 163.8 eV which could be assigned to the S 2p1/2 and S 2p3/2 in dibenzothiophene units, respectively [51]. In P-FSO and P-FSOF, these two peaks shift to about 168.8 and 167.5 eV which are related to the S species in sulphonyl groups [51]. In addition, elemental analysis of these polymers also supports the structures as proposed (Table S1).

The surface morphologies of polymers were characterized using SEM. As displayed in Fig. S3, all of them have a fused particle-like shape

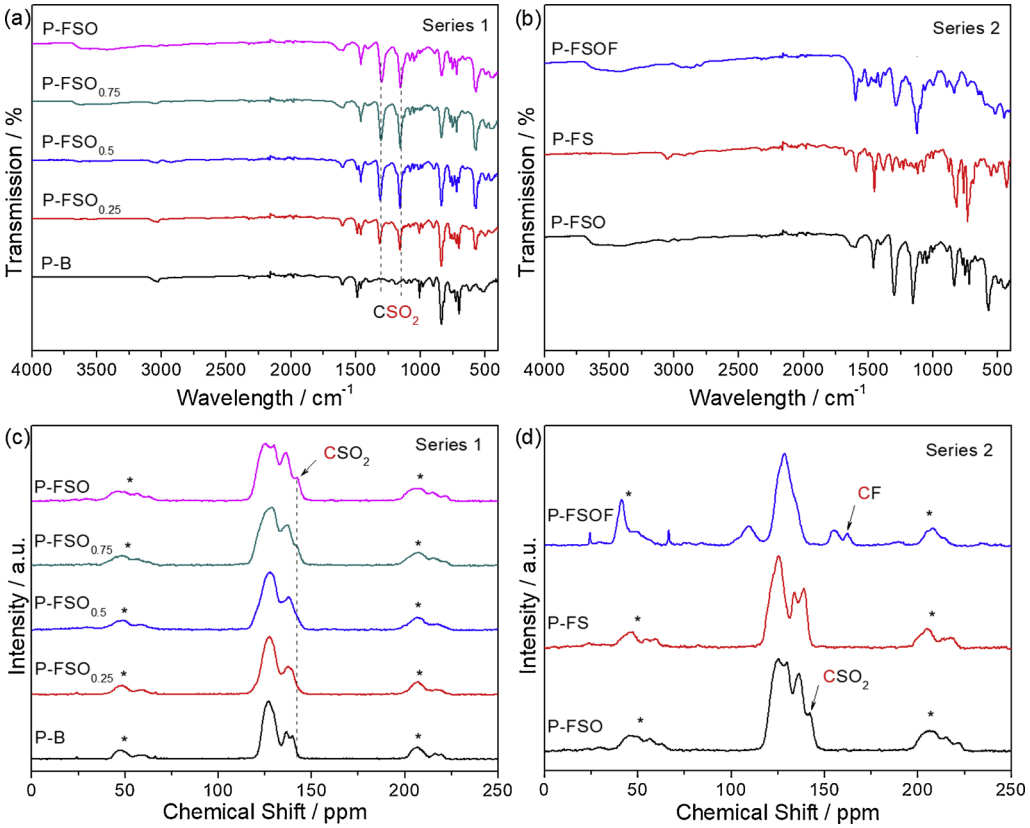

Fig. 2. FT-IR spectra (a, b) and Solid-stated ^{13}C NMR spectra (c, d) of polymers.

Table 1
Surface areas, photophysical properties and photocatalytic performance of the polymers.

Polymer	S_{BET}[a] [$m^2 g^{-1}$]	OG[b] [eV]	$SUM_{charges}$-P[c] [e]	HER[d] [μmol h^{-1}]
P-B	724	2.53	0.13	4
P-$FSO_{0.25}$	585	2.45	0.20	70
P-$FSO_{0.5}$	467	2.41	0.27	189
P-$FSO_{0.75}$	431	2.37	0.33	356
P-FSO	492	2.31	0.38	400
P-FS	236	2.48	0.16	1
P-FSOF	865	2.32	0.63	7

[a] Specific surface area were calculated from the N_2 adsorption isotherm.
[b] Optical gap (OG) was derived from the absorption edge.
[c] The sum of Mulliken atomic charges of all pyrene units ($SUM_{charges}$-P) in each polymer from DFT calculation.
[d] Reaction conditions: polymer (50 mg), TEOA/H_2O (1/10 in vol, 110 mL), 300 W Xe lamp with cut-off filter > 420 nm.

except for P-FS which forms a fused rod-like shape. This obvious difference in surface morphology directly influences the porosity of polymers. The fused particle-like polymers are more porous to nitrogen at 77 K, with apparent Brunauer-Emmett-Teller surface areas (S_{BET}) between 431 and 865 $m^2 g^{-1}$ and the P-FSOF has the best porosity as shown in Table 1 (for more detailed porosity data see the Fig. S4 and Table S2). By contrast, the BET surface area of fused rod-like P-FS significantly decreases to a value of 236 $m^2 g^{-1}$. It is also obvious that, all the FSO-containing polymers in Series 1 possess lower porosity (S_{BET}: 431 to 585 $m^2 g^{-1}$) than P-B (S_{BET}: 724 $m^2 g^{-1}$), which is not beneficial for photocatalytic performance.

DFT caculations of fragmental structures (see Fig. S5) of polymers were carried out to gain insightful information, not only the HOMO/LUMO levels but also about the Mulliken atomic charges in each polymer can be achieved. As shown in Fig. 3a, the LUMO levels of polymers ranging from -2.46 to -3.07 eV are all able to drive the hydrogen evolution reaction with the sufficient enough over-potentials higher than 1.37 V. Further calculation of Mulliken atomic charges in each polymer was performed. Since the sum of charges of all atoms in each polymer structure is 0.00 e, we can use the sum of charges of all pyrene units ($SUM_{charges}$-P) in each polymer to quantize the electron withdrawing ability of different acceptors. For instance, in the fragmental structure of P-FSO (Fig. 3b), we can get the Mulliken atomic charges of every atom from DFT calculation as depicted in Fig. 3c, and the value of the $SUM_{charges}$-P could be calculated to be 0.38 e by summing the charges of all atoms in P1 - P5. As shown in Table 1, the other polymers also exhibit the positive values of $SUM_{charges}$-P suggesting the delocalization of electrons from pyrene to acceptor, and here, the higher value of $SUM_{charges}$-P means the stronger electron withdrawing ability of acceptor in polymer structure. It is obvious that, for FSO containing polymers, the higher FSO content, the higher value of $SUM_{charges}$-P is present and the O atom has the lowest value of Mulliken atomic charges (Fig. 3c) proving the highest concentration of electron on O atoms. Moreover, the value of $SUM_{charges}$-P in P-FSOF is greatly larger than others, even the P-FSO, which indicates the outstanding electron-capture ability of additional F atoms in P-FSOF.

To achieve an effective photocatalytic performance, proper optical gaps are required for the photocatalysts. Herein, this property of all the prepared polymers was investigated by UV–vis diffuse reflectance spectra (UV/Vis DRS). As shown in the UV/Vis DRS spectra (Fig. 4a), all the polymers display the good absorption range in visible region. For the polymers in Series 1, a red-shift of the absorption edge in the UV/Vis DRS spectra is observed when the FSO content enhances in the polymer structure. This is probably because of the extended π-conjugation degree for FSO than benzene. Optical gaps for these polymers between 2.53 and 2.31 eV (Table 1) could be calculated from their absorption edges. In Series 2, the P-FSOF exhibits an optical gap of 2.32 eV which is nearly identical with P-FSO. However, the P-FS has a

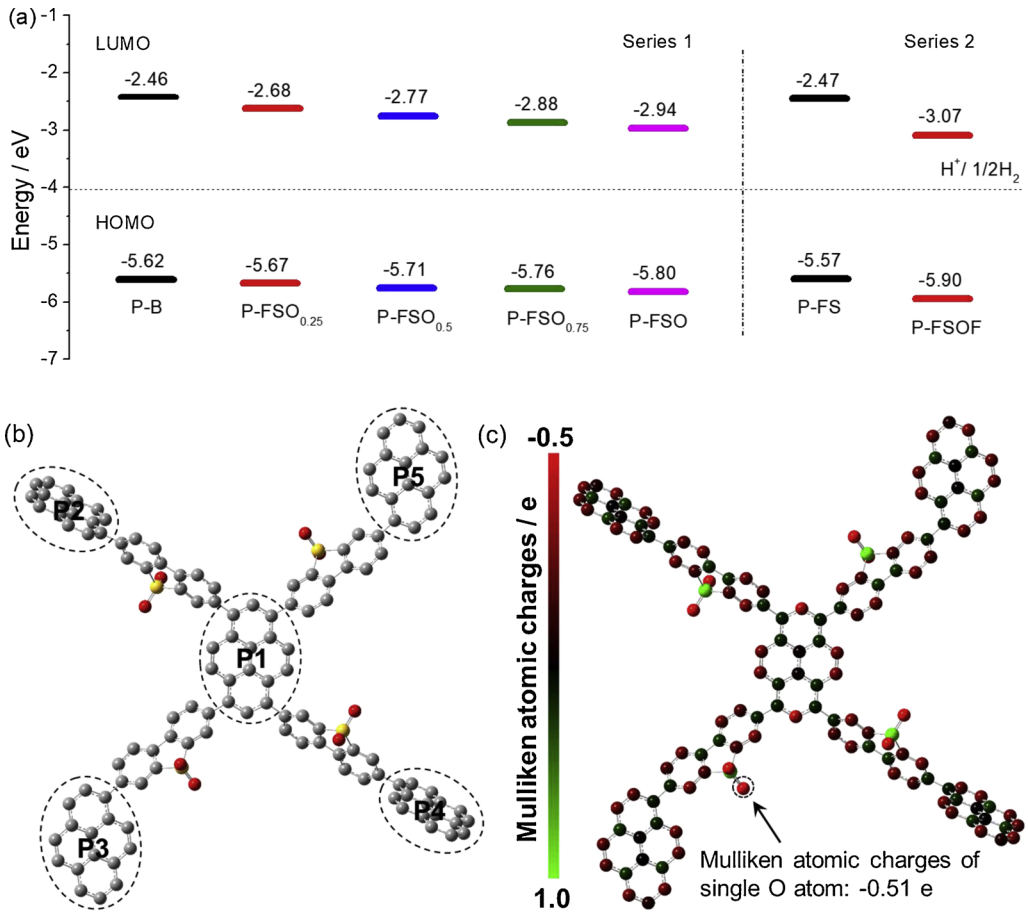

Fig. 3. a) The theoretical band gap of fragmental structures of polymers from DFT calculations. b Optimized fragmental structure of P-FSO from DFT calculation (Grey: C; Red: O; Yellow: S). c) Mulliken atomic charges of every atom in P-FSO. (For interpretation of the references to colour in this figure legend, the reader is referred to the web version of this article).

much broader optical gap of 2.48 eV than P-FSO and P-FSOF, but still narrower than P-B (2.53 eV).

The photoluminescence spectra (PL) of all polymers are displayed in Fig. 4b. It is clear that all the polymers present totally different emission peaks and the wavelength of emission peak for each polymer is highly corresponding to its wavelength of absorption edge in the UV/Vis DRS spectra, further certifying the different band-gap energy of each polymer. Furthermore, by gradually changing the FSO contents in Series 1, the stronger photoluminescence quenching is realized. It indicates that the depopulation of the excitons through radiative pathways become more difficult, presumably by intramolecular charge transfer (ICT) from donor to acceptor, and thus point to the improved charge separation. For the polymers in Series 2, the P-FSOF shows a weakest fluorescence emission peak which is probably due to FSOF is a much stronger acceptor than FSO, so that the ICT in P-FSOF is most prominent, which has already been well identified by DFT calculation. From the further time-resolved PL measurements, we can find that all the prepared polymers display a limited PL lifetime (average PL lifetimes varying from 1.54 to 2.81 ns, see Fig. S8), which is also observed in other conjugated polymer photocatalysts [52–54]. This is a reminder that even the dissociation of photogenerated excitons could be enhanced by ICT in D-A polymer, the separated elections still may be fast quenched by other pathways, which highlights the importance of efficient electron-output ability of D-A polymer photocatalyst during photocatalytic reaction.

The photocatalytic performance of all prepared polymers in hydrogen evolution from water was determined in the presence of triethanolamine (TEOA) as a sacrificial electron donor. It is already well

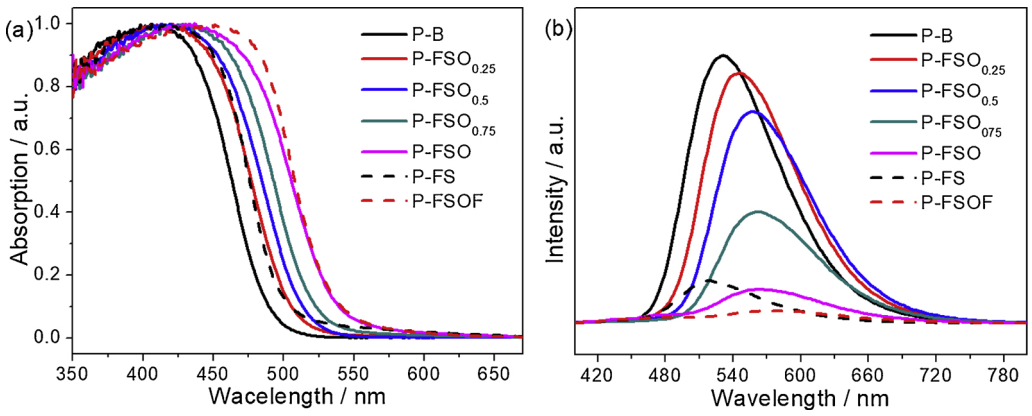

Fig. 4. a) UV/Vis diffuse reflectance spectra (DRS) of polymers. b) Photoluminescence spectra of polymers measured in the solid-state powder ($\lambda_{excitation}$ = 295 nm).

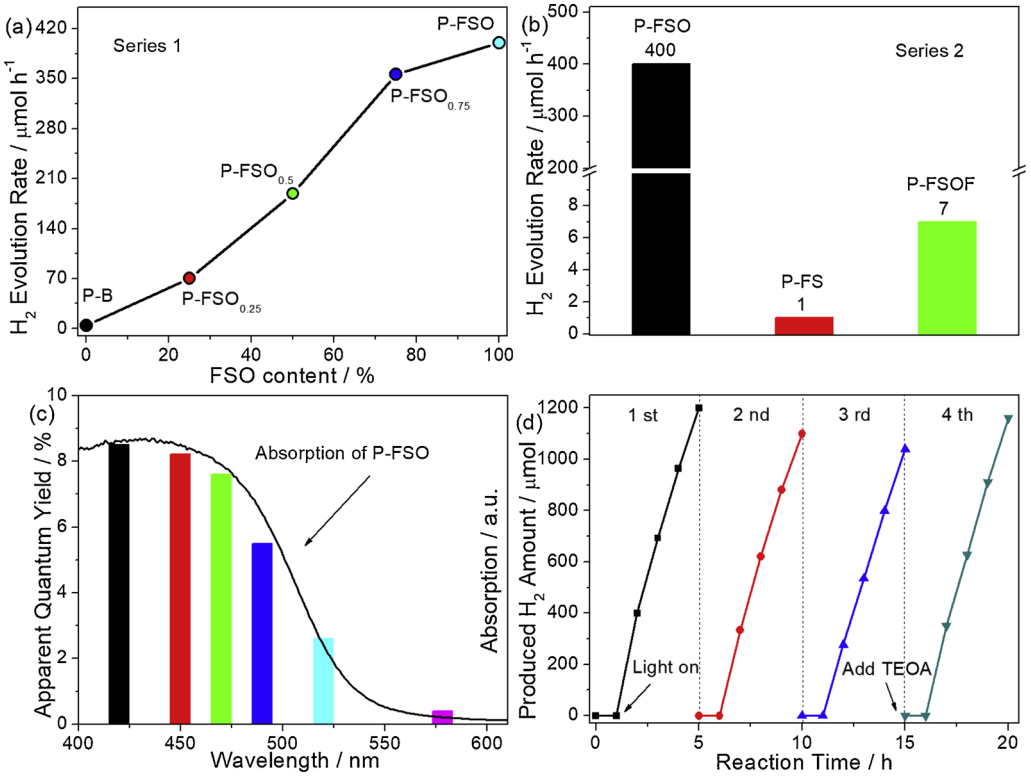

Fig. 5. H_2 evolution rates under visible-light irradiation ($\lambda > 420$ nm) using polymers in Series 1 (a) and Series 2 (b). c) Wavelength dependence of AQY on H_2 evolution using P-FSO. d) Stability and reusability test using P-FSO as a photocatalyst under visible-light irradiation ($\lambda > 420$ nm).

known that the residual palladium in these polymers (Pd Content: ~1.0 wt.%, see Table S3) can efficiently act as a co-catalyst [26,31,36]. Hence, all the polymers were tested without adding any additional metal co-catalyst (e.g., Pt). As displayed in Fig. 5a and b, among all polymers, P-FSO gives the best photocatalytic performance with a HER of 400 μmol h^{-1} under visible light irradiation ($\lambda > 420$ nm) and an apparent quantum yield (AQY) of 8.5% at 420 nm. In addition, from the data of wavelength dependence of AQY on hydrogen evolution using P-FSO shown in Fig. 5c, we can find a well match between the AQYs of hydrogen evolution and UV/Vis absorption spectrum, which indicates that the reaction is indeed triggered by light irradiation. Moreover, the P-FSO also represents a good stability as photocatalyst which can keep the HER in 25 h without loss in the photocatalytic efficiency, by maintaining the original concentration of sacrificial agent (Fig. 5d) and no apparent change could be found in the XRD, FTIR and ^{13}C NMR results of the recycled catalysts (Fig. S9).

Aside from P-FSO, the other FSO-containing polymers in Series 1 also exhibit much better photocatalytic performance than P-B and it is easy to figure out that by gradually increasing the FSO content in the structure, the HER of the polymers increases step by step. This trend is consistent with the light absorption ability and exciton-separation efficiency. However, as the significant difference between P-B and P-FSO in HER, it is much probable that the FSO in the polymer structure not only benefits for improving the light absorption ability and exciton-separation efficiency, but also can greatly helpful for outputting the electrons to the co-catalyst or proton to drive the reaction. Herein, considering of the distribution of Mulliken atomic charges, we presume that the sulphonyl group in FSO may serve as the electron-output "tentacle".

To verify this hypothesis, the H atom adsorption free energy (ΔG_H), which is accredited as an appropriate descriptor for hydrogen evolution reaction [55,56], has been investigated by DFT based calculations. It is generally accepted that the optimum value should be around $\Delta G_H = 0$ eV and the transition-metal Pd exhibits a good value of $\Delta G_H = -0.2$ eV, approximately, which could be an efficient co-catalyst [55]. To simplify the calculations, we use the oligomeric structures (Fig. S10) instead of the polymeric structures and ΔG_H was calculated for single H atom adsorbed on heteroatom sites in P-FSO, P-FS and P-FSOF.

As shown in Fig. 6a, it is obvious that ΔG_H at different heteroatom sites are significantly different. The ΔG_H at sulfur site in P-FS is 2.23 eV and at fluorine site in P-FSOF is 2.26 eV, respectively, which means a large overpotential for hydrogen evolution. Among all these heteroatom sites, the oxygen site in sulphonyl group exhibits the best value of ΔG_H, namely, 1.66 and 1.74 eV in P-FSO and P-FSOF, respectively. Whereas, the value of ΔG_H at oxygen site is still much higher than it at Pd site suggesting that Pd co-catalyst is the thermodynamically favored site for hydrogen evolution reaction, which is in accord with previous report [57].

Since the vital role of co-catalyst in protons reduction, we further used DFT calculations to explore the interaction between Pd and different heteroatom sites in each polymer structure. After considering Pd absorbed at different heteroatom sites, different Mulliken atomic charges value for Pd are generated. This is caused by the different interactions between Pd and heteroatoms and the negative value of charge means the heteroatom can output the electrons to Pd co-catalyst. As shown in Fig. 6b, only being absorbed at sulfur site in P-FS and oxygen site in P-FSO, the Pd can receive electrons from polymer structure which is requisite for driving the photocatalytic protons reduction.

All these results reveal that no matter the protons are directly reduced at heteroatom site in polymer or reduced at co-catalyst, the sulphonyl group in P-FSO is most thermodynamically efficient electron-output unit during the photocatalytic reaction. This conclusion can well explain the significant difference in HER between P-FSO and P-FS or P-

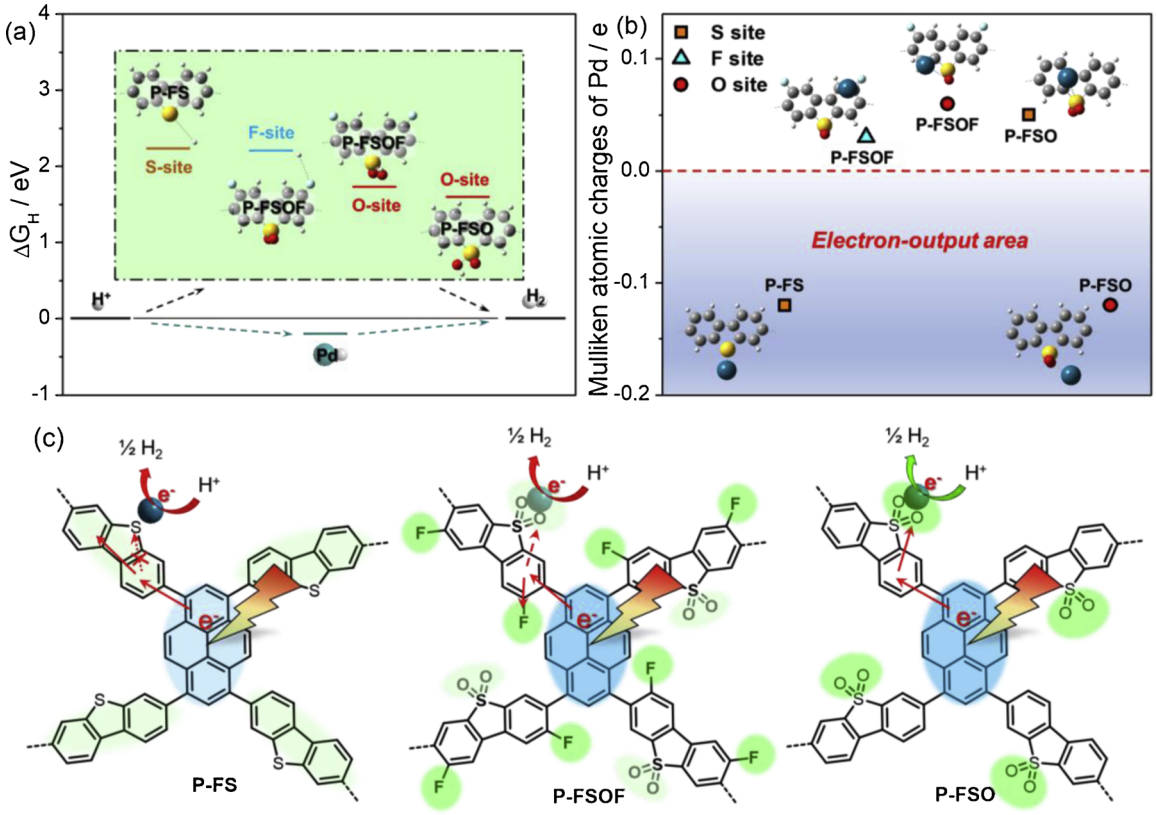

Fig. 6. a) Hydrogen adsorption free energy, ΔG_H, at oxygen, sulfur and fluorine sites - the case of one hydrogen atom. b) Mulliken atomic charges of palladium atom after being absorbed at oxygen, sulfur or fluorine sites. c) The speculative photoelectron transfer pathway in P-FS, P-FSOF and P-FSO.

FSOF. To make a clear illumination, the photoelectron transfer pathway in these three polymers are speculated and displayed in Fig. 6c. For P-FS, the absence of sulphonyl group leads to the decrease of light absorption ability and the most probably electron output site, sulfur site, cannot efficiently concentrate the photogenerated electrons even it has a well interaction with co-catalyst. The P-FSOF contains the sulphonyl group, however, the two strongly electrophilic F atoms can significantly enhance the electron withdrawing ability of FSOF unit which has been identified by DFT calculations, so that electrons could not be delivered to co-catalyst readily. Only P-FSO, in which the sulphonyl group can efficiently concentrate as well as output electrons, successfully builds the perfectly electron-output "tentacle" and represents an excellent hydrogen evolution performance.

Furthermore, the analogues of P-B and P-FSO, two linear polymers (L-P-B and L-P-FSO), were synthesized to study the effect of electron-output "tentacle" on photocatalytic performance in different nanostructure (Fig. 7a). As shown in Fig. 7b, the L-P-B cannot generate hydrogen from water, whereas, the L-P-FSO shows a HER of 20 μmol h^{-1}. This significant improvement in HER further verifies the importance of electron-output "tentacle".

4. Conclusions

In conclusion, we design a series of D-A conjugated polymer photocatalysts for efficient hydrogen evolution, in which the presence of dibenzothiophene-*S,S*-dioxide (FSO) units can greatly optimize the light absorption ability and exciton-separation efficiency as well as perfectly act as an electron-output "tentacle". Among them, P-FSO demonstrates a fabulous photocatalytic efficiency for conjugated polymers with a HER of 400 μmol h^{-1} ($\lambda > 420$ nm) and an apparent quantum yield (AQY) of 8.5% at 420 nm using triethanolamine (TEOA) as the sacrificial agent and without any additional metal co-catalyst (e.g., Pt). DFT calculations suggest that sulphonyl group is an important electron-output unit during the photocatalytic reaction. Further deeply analyzing the significant difference in HER between P-FSO and P-FS or P-FSOF, we find that only P-FSO, in which the sulphonyl group can

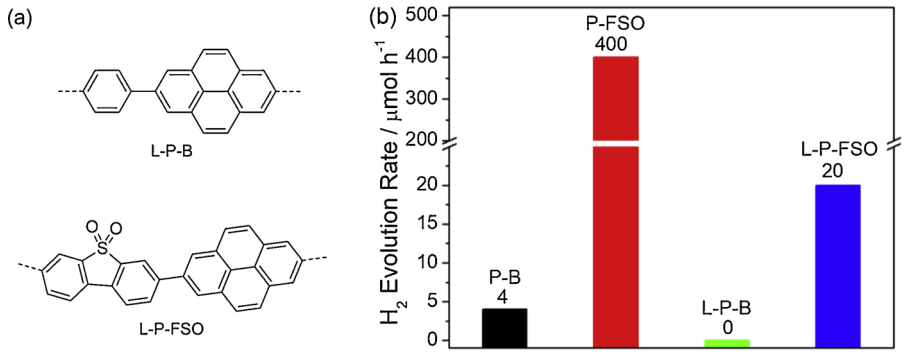

Fig. 7. Molecular structures (a) and H_2 evolution rates (b) of two synthesized liner polymers.

efficiently concentrate as well as output electrons, successfully builds the perfect electron-output “tentacle”, resulting in an excellent hydrogen evolution performance. This study highlights the importance of electron-output ability in photocatalytic process and offers a promising strategy to rationally design conjugated polymer photocatalyst with electron-output “tentacle”. Through this strategy, there is a high potential for further optimization of polymer structure to obtain a more efficient hydrogen evolution performance, even to achieve the overall water splitting without any sacrificial agents.

Acknowledgments

This work was financially supported by the National Natural Science Foundation of China (21761132002, 21425309 and 21861130353), the National Basic Research Program of China (2013CB632405), the National Key Technologies R & D Program of China (2018YFA0209301), the 111 Project (D16008) and the scholarship from China Scholarship Council (CSC) (No. 201706650004).

Appendix A. Supplementary data

Supplementary material related to this article can be found, in the online version, at doi:https://doi.org/10.1016/j.apcatb.2019.01.010.

References

[1] V.S. Vyas, B.V. Lotsch, Nature 521 (2015) 41–42.
[2] C. Huang, C. Chen, M. Zhang, L. Lin, X. Ye, S. Lin, M. Antonietti, X. Wang, Nat. Commun. 6 (2015) 7698.
[3] Y. Fang, X. Wang, Angew. Chem. Int. Ed. 56 (2017) 15506–15518.
[4] M. Zheng, J. Shi, T. Yuan, X. Wang, Angew. Chem. Int. Ed. 57 (2018) 5487–5491.
[5] T. Shao, Z. Jiang, Acta Chim. Sin. 75 (2017) 70–73.
[6] L. Chen, M. Zhou, Z. Luo, M. Wakeel, A.M. Asiri, X. Wang, Appl. Catal. B: Environ. 241 (2019) 246–255.
[7] Y. Qu, N. Sun, M. Humayun, A. Zada, Y. Xie, J. Tang, L. Jing, H. Fu, Sustain. Energy Fuels 2 (2018) 549–552.
[8] A. Kudo, Y. Miseki, Chem. Soc. Rev. 38 (2009) 253–278.
[9] J. Wu, Z. Ji, X. Shen, X. Miao, K. Xu, Acta Chim. Sinica 75 (2017) 1207–1214.
[10] D. Liu, W. Cai, Y. Wang, Y. Zhu, Appl. Catal. B: Environ. 236 (2018) 205–211.
[11] X. Wang, K. Maeda, A. Thomas, K. Takanabe, G. Xin, J.M. Carlsson, K. Domen, M. Antonietti, Nat. Mater. 8 (2009) 76–80.
[12] Y. Zheng, L. Lin, B. Wang, X. Wang, Angew. Chem. Int. Ed. 54 (2015) 12868–12884.
[13] Z.A. Lan, G. Zhang, X. Wang, Appl. Catal. B: Environ. 92 (2016) 116–125.
[14] L. Lin, H. Ou, Y. Zhang, X. Wang, ACS Catal. 6 (2016) 3921–3931.
[15] G. Zhang, G. Li, Z.A. Lan, L. Lin, A. Savateev, T. Heil, S. Zafeiratos, X. Wang, M. Antonietti, Angew. Chem. Int. Ed. 56 (2017) 13445–13449.
[16] M. Zhou, Z. Hou, L. Zhang, Y. Liu, Q. Gao, X. Chen, Sustain. Energy Fuels 1 (2017) 317–323.
[17] G. Zhang, L. Lin, G. Li, Y. Zhang, A. Savateev, S. Zafeiratos, X. Wang, M. Antonietti, Angew. Chem. Int. Ed. 57 (2018) 9372–9376.
[18] L. Lin, W. Ren, C. Wang, A.M. Asiric, J. Zhang, X. Wang, Appl. Catal. B: Environ. 231 (2018) 234–241.
[19] L. Lin, C. Wang, W. Ren, H. Ou, Y. Zhang, X. Wang, Chem. Sci. 8 (2017) 5506–5511.
[20] W.J. Ong, L.L. Tan, Y.H. Ng, S.T. Yong, S.P. Chai, Chem. Rev. 116 (2016) 7159–7329.
[21] G. Zhang, Z.-A. Lan, X. Wang, Angew. Chem. Int. Ed. 55 (2016) 15712–15727.
[22] R.S. Sprick, L. Wilbraham, Y. Bai, P. Guiglion, A. Monti, R. Clowes, A.I. Cooper, M.A. Zwijnenburg, Chem. Mater. 30 (2018) 5733–5742.
[23] D.J. Woods, R.S. Sprick, C.L. Smith, A.J. Cowan, A.I. Cooper, Adv. Energy Mater. 7 (2017) 1700479.
[24] R.S. Sprick, C.M. Aitchison, E. Berardo, L. Turcani, L. Wilbraham, B.M. Alston, K.E. Jelfs, M.A. Zwijnenburg, A.I. Cooper, J. Mater. Chem. A 6 (2018) 11994–12003.
[25] J. Xie, S.A. Shevlin, Q. Ruan, S.J.A. Moniz, Y. Liu, X. Liu, Y. Li, C.C. Lau, Z.X. Guo, J. Tang, Energy Environ. Sci. 11 (2018) 1617–1624.
[26] R.S. Sprick, J.X. Jiang, B. Bonillo, S. Ren, T. Ratvijitvech, P. Guiglion, M.A. Zwijnenburg, D.J. Adams, A.I. Cooper, J. Am. Chem. Soc. 137 (2015) 3265–3270.
[27] N. Banerji, S. Cowan, M. Leclerc, E. Vauthey, A.J. Heeger, J. Am. Chem. Soc. 132 (2010) 17459–17470.
[28] B.S. Rolczynski, J.M. Szarko, H.J. Son, Y. Liang, L. Yu, L.X. Chen, J. Am. Chem. Soc. 134 (2012) 4142–4152.
[29] K.W. Wang, L.M. Yang, X. Wang, L.P. Guo, G. Cheng, C. Zhang, Sb. Jin, B. Tan, A. Cooper, Angew. Chem. Int. Ed. 56 (2017) 14149–14153.
[30] Z.A. Lan, Y. Fang, Y. Zhang, X. Wang, Angew. Chem. Int. Ed. 57 (2018) 470–474.
[31] R.S. Sprick, B. Bonillo, R. Clowes, P. Guiglion, N.J. Brownbill, B.J. Slater, F. Blanc, M.A. Zwijnenburg, D.J. Adams, A.I. Cooper, Angew. Chem. Int. Ed. 55 (2016) 1792–1796.
[32] C. Yang, B.C. Ma, L.Z. Zhang, S. Lin, S. Ghasimi, K. Landfester, K.A.I. Zhang, X.C. Wang, Angew. Chem. Int. Ed. 55 (2016) 9202–9206.
[33] Y. Fu, X. Zhu, L. Huang, X. Zhang, F. Zhang, W. Zhu, Appl. Catal. B: Environ. 239 (2018) 46–51.
[34] H. Ou, X. Chen, L. Lin, Y. Fang, X. Wang, Angew. Chem. Int. Ed. 57 (2018) 8729–8733.
[35] Y.S. Kochergin, D. Schwarz, A. Acharjya, A. Ichangi, R. Kulkarni, P. Eliášová, J. Vacek, J. Schmidt, A. Thomas, M.J. Bojdys, Angew. Chem. Int.Ed. 57 (2018) 14188–14192.
[36] L.W. Li, Z.X. Cai, Q.H. Wu, W.Y. Lo, N. Zhang, L.X. Chen, L.P. Yu, J. Am. Chem. Soc. 138 (2016) 7681–7686.
[37] P.B. Pati, G. Damas, L. Tian, D.L.A. Fernandes, L. Zhang, I.B. Pehlivan, T. Edvinsson, C.M. Araujo, H. Tian, Energy Environ. Sci. 10 (2017) 1372–1376.
[38] T.H. Huang, W.T. Whang, J.Y. Shen, Y.S. Wen, J.T. Lin, T.H. Ke, L.Y. Chen, C.C. Wu, Adv. Funct. Mater. 16 (2006) 1449–1456.
[39] L. Yu, J. Liu, S. Hu, R. He, W. Yang, H. Wu, J. Peng, R. Xia, D.D.C. Bradley, Adv. Funct. Mater. 23 (2013) 4366–4376.
[40] X. Wang, L. Chen, S.Y. Chong, M.A. Little, Y. Wu, W.H. Zhu, R. Clowes, Y. Yan, M.A. Zwijnenburg, R.S. Sprick, A.I. Cooper, Nat. Chem. 10 (2018) 1180–1189.
[41] C. Dai, S. Xu, W. Liu, X. Gong, M. Panahandeh-Fard, Z. Liu, D. Zhang, C. Xue, K.P. Loh, B. Liu, Small 14 (2018) 1801839.
[42] Z. Wang, X. Yang, T. Yang, Y. Zhao, F. Wang, Y. Chen, J.H. Zeng, C. Yan, F. Huang, J.X. Jiang, ACS Catal. 8 (2018) 8590–8596.
[43] Y. Zhao, W. Ma, Y. Xu, C. Zhang, Q. Wang, T. Yang, X. Gao, F. Wang, C. Yan, J.X. Jiang, Macromolecules 51 (2018) 9502–9508.
[44] K.H. Lee, K. Morino, A. Sudo, T. Endo, Polym. Bull. 67 (2011) 227–236.
[45] K.C. Moss, K.N. Bourdakos, V. Bhalla, K.T. Kamtekar, M.R. Bryce, M.A. Fox, H.L. Vaughan, F.B. Dias, A.P. Monkman, J. Org. Chem. 75 (2010) 6771–6781.
[46] J.S. Ward, R.S. Nobuyasu, A.S. Batsanov, P. Data, A.P. Monkman, F.B. Diasb, M.R. Bryce, Chem. Commun. 52 (2016) 2612–2615.
[47] H. Li, A.S. Batsanov, K.C. Moss, H.L. Vaughan, F.B. Dias, K.T. Kamtekar, M.R. Bryce, A.P. Monkman, Chem. Commun. 46 (2010) 4812–4814.
[48] S. Sasaki, S. Suzuki, K. Igawa, K. Morokuma, G.I. Konishi, J. Org. Chem. 82 (2017) 6865–6873.
[49] M.J. Frisch, G.W. Trucks, H.B. Schlegel, G.E. Scuseria, M.A. Robb, J.R. Cheeseman, J.A. Montgomery Jr, T. Vreven, K.N. Kudin, J.C. Burant, J.M. Millam, S.S. Iyengar, J. Tomasi, V. Barone, B. Mennucci, M. Cossi, G. Scalmani, N. Rega, G.A. Petersson, H. Nakatsuji, M. Hada, M. Ehara, K. Toyota, R. Fukuda, J. Hasegawa, M. Ishida, T. Nakajima, Y. Honda, O. Kitao, H. Nakai, M. Klene, X. Li, J.E. Knox, H.P. Hratchian, J.B. Cross, V. Bakken, C. Adamo, J. Jaramillo, R. Gomperts, R.E. Stratmann, O. Yazyev, A.J. Austin, R. Cammi, C. Pomelli, J.W. Ochterski, P.Y. Ayala, K. Morokuma, G.A. Voth, P. Salvador, J.J. Dannenberg, V.G. Zakrzewski, S. Dapprich, A.D. Daniels, M.C. Strain, O. Farkas, D.K. Malick, A.D. Rabuck, K. Raghavachari, J.B. Foresman, J.V. Ortiz, Q. Cui, A.G. Baboul, S. Clifford, J. Cioslowski, B.B. Stefanov, G. Liu, A. Liashenko, P. Piskorz, I. Komaromi, R.L. Martin, D.J. Fox, T. Keith, M.A. Al-Laham, C.Y. Peng, A. Nanayakkara, M. Challacombe, P.M.W. Gill, B. Johnson, W. Chen, M.W. Wong, C. Gonzalez, J.A. Pople, Gaussian 03, Revision D.01, Gaussian, Inc., Wallingford CT, 2004.
[50] B. Lu, Y. Li, J. Xu, J. Electroanal. Chem. 643 (2010) 67–76.
[51] S.R. Kelemen, G.N. George, M.L. Gorbaty, Fuel 69 (1990) 939–944.
[52] Y. Xu, N. Mao, C. Zhang, X. Wang, J. Zeng, Y. Chen, F. Wang, J.X. Jiang, Appl. Catal. B: Environ. 228 (2018) 1–9.
[53] Y. Xu, C. Zhang, P. Mu, N. Mao, X. Wang, Q. He, F. Wang, J.X. Jiang, Sci. China Chem. 60 (2017) 1075–1083.
[54] Y. Xu, N. Mao, S. Feng, C. Zhang, F. Wang, Y. Chen, J. Zeng, J.X. Jiang, Macromol. Chem. Phys. 218 (2017) 1700049.
[55] J. Greeley, T.F. Jaramillo, J. Bonde, I. Chorkendorff, J.K. Norskov, Nat. Mater. 5 (2006) 909–913.
[56] H. Li, C. Tsai, A.L. Koh, L. Cai, A.W. Contryman, A.H. Fragapane, J. Zhao, H.S. Han, H.C. Manoharan, F. Abild-Pedersen, J.K. Norskov, X. Zheng, Nat. Mater. 15 (2016) 48–53.
[57] G. Zhang, Z.A. Lan, X. Wang, Chem. Sci. 8 (2017) 5261–5274.